JACS
JOURNAL OF THE AMERICAN CHEMICAL SOCIETY

Article

pubs.acs.org/JACS

Building Nanowires from Micelles: Hierarchical Self-Assembly of Alternating Amphiphilic Glycopolypeptide Brushes with Pendants of High-Mannose Glycodendron and Oligophenylalanine

Yijiang Liu, Yufei Zhang, Zheyu Wang, Jue Wang, Kongchang Wei, Guosong Chen,* and Ming Jiang

The State Key Laboratory of Molecular Engineering of Polymers and Department of Macromolecular Science, Fudan University, Shanghai 200433, China

Supporting Information

ABSTRACT: Mimicking the diverse glyco-conjugate structures in nature is always the dream of scientists. Right now, hierarchical self-assembled structures of natural conjugates of peptides and sugars could not easily be achieved via linear glycopolypeptide with monosaccharides as attachments. In this work, by using a series of well-designed alternating amphiphilic glycopolypeptide brushes (AAGBs) with pendants of glycodendrons and short peptides, various self-assembled morphologies were achieved, including nanowires, nanoribbon, and compound micelles mainly depending on the number ratio of the sugar units to the amino acids species (S/F). Among these morphologies, nanowire attracted our great attention. TEM studies demonstrated that it is formed via a hierarchical self-assembly, i.e., a series of successive processes, including micellization, micelles alignment forming nanofilament, branching of the nanofilaments by micelles, and finally nanowire formation. As far as we know, such hierarchical self-assembly process with high complexity has not been observed in literature for glycopolypeptides even polypeptides, which will deepen our understanding on self-assembly mechanism of natural glyco-conjugates and expand the library of biomimetic materials.

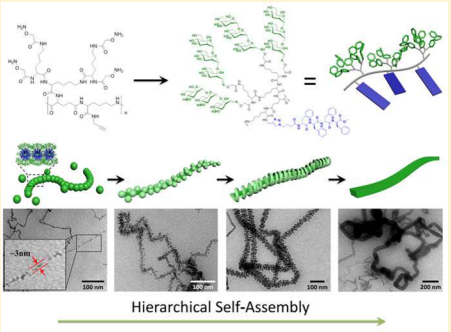

INTRODUCTION

In nature, saccharides and peptides are often covalently connected to each other forming various biomacromolar conjugates,[1] such as glycoproteins, mucins, and proteoglycans, which can form a variety of assembled structures especially hierarchical ones,[2] including micelles, vesicles, worm-like micelles, nanowires, nanoribbons, etc.[3] These self-assembled structures play key roles in a broad range of biological processes including modulating intercellular communication,[4] cell adhesion,[5] and immunological recognition.[6] In the past decade, significant progress on bioinspired synthetic glyco-peptides[7] have been achieved via different approaches aiming at mimicking the functions of the native ones[8] and developing new biocompatible materials.[9] Among these mimics, glycopolypeptide[10] prepared by ring-opening polymerization is a promising one, featured by facile preparation and easy scale-up.[11] In this field, artificial glycopolypeptides with a polypeptide backbone and monosaccharides as pendent groups were prepared by controlled polymerization[12] and, in some cases, followed by postpolymerization modification.[13] In these artificial glycopolypeptide systems, the carbohydrates not only contribute to the bioavailability[14] but also modulate the folding[15] and the self-assembly[16] of the conjugates. However, among these elegant works in the past, very different from the architectural varieties of their native counterparts, the artificial glycopolypeptides studied were mainly focusing on linear or linear-branched[17] block copolymers, which usually led to zero dimentional structures,[18] e.g., micelles and vesicles exclusively. Thus, these limitations hamper our understanding on the self-assembly mechanism of native glyco-conjugates[19] as well as the development of functional biomaterials based on glycopolypeptides for drug delivery,[20] bioimaging,[21] tissue engineering,[22] etc.

Aiming at creating more abundant morphologies, especially the hierarchical self-assembled ones from artificial glycopolypeptides approaching to those in nature, in this work we tried a new type of glycopolypeptide, prepared by postpolymerization modification of a polypeptide backbone with oligosaccharide and oligopeptide as pendent brushes. The obtained new polymer is featured by the alternating amphiphilic brushes of dendronized oligosaccharides and oligopeptides along the polymeric peptide backbone. It is well-known that polymer brushes, particularly amphiphilic polymer brushes, being a family of new architectures of copolymers have drawn great attention in the last 2 decades[23] as their relatively well-defined structures provide broad opportunities to control hydrophobic−hydrophilic balance and then the final assemblies. However, in most cases their assemblies possess lamellar structure as the result of phase separation of the side chains to opposite sides of the polymer backbone. Some recent works introduce crystallizable chains,[24] liquid crystal[25] or bulky POSS[26] as brushes but did not bring out new findings in self-assembly. It is also well-known that short peptides are excellent building blocks to create a wide variety of nanostructures,[27]

Received: May 16, 2016
Published: July 22, 2016

DOI: 10.1021/jacs.6b05044
J. Am. Chem. Soc. 2016, 138, 12387−12394

Scheme 1. Synthetic Routes and Chemical Structures of Dendritic Polypeptide Scaffolds P0, P1, and P2

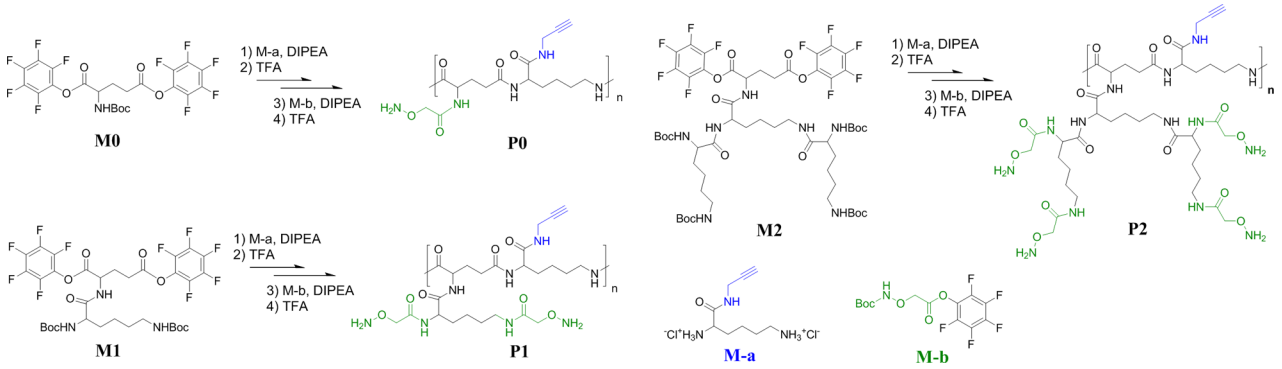

Scheme 2. Synthesis and Chemical Structures of (a) Alternating Amphiphilic Glycopolypeptide Brush (AAGB) P2tM-F_4, (b) Full Space Model, and (c) 3D Schematic Illustration of the Repeating Unit of P2tM-F_4

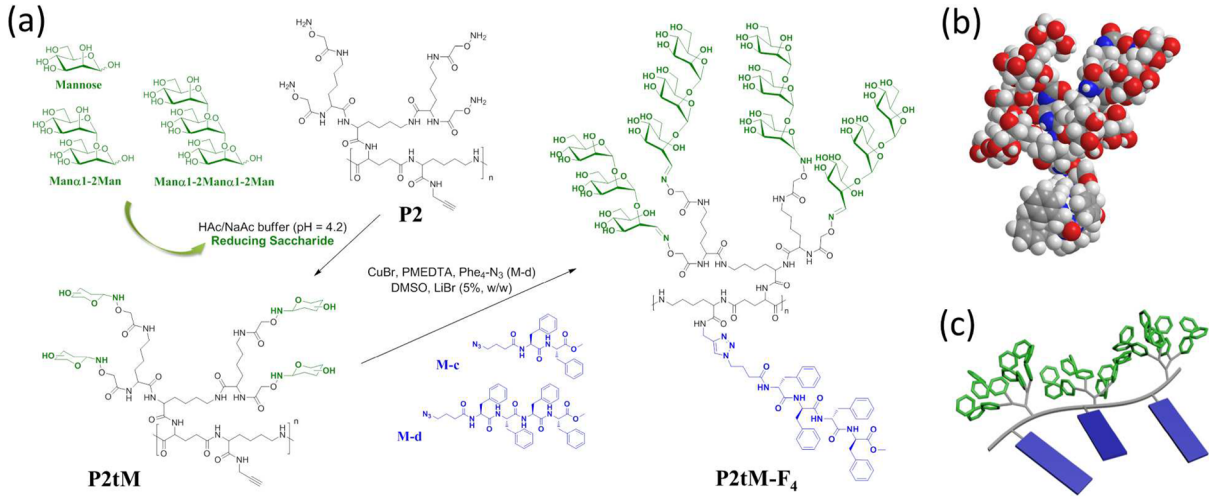

some of which, such as nanowire,[28] nanoribbon,[29] resembles those in nature.[30,31] However, such strong assembly ability of peptide leading to morphologies found in nature has rarely recurred in brush polymers with peptide as side chains and even less in glycopolypeptides.[32]

In our design, the glycodendron attachment makes the conjugates unique in a very high density of sugar units, of which carbohydrate−carbohydrate interaction[33] may promote assembly of the conjugates; meanwhile, the pendent β-sheet forming oligopeptide is expected to provide the driving force for the assembly resembling that occurring in nature. Thus, new glycopolypeptide architecture, i.e., alternating amphiphilic glycopeptide brushes (AAGBs) was prepared by modification of Manα1-2Man oligomannosides and oligophenylalanines to the lysine/glutamate based dendritic backbone.[34] Manα1-2Man was selected because this structure was highly expressed on the surface of virus and bacteria, e.g., gp120,[35] a major envelope protein of HIV, which could be recognized by human monoclonal antibody (mAbs) 2G12.[36]

Meanwhile, the oligophenylalanine (L-Phe_n, FF, or FFFF) extracted from the Alzheimer's β-amyloid polypeptide,[37] was found to have an excellent capacity in forming a wide range of nanostructures.[38] To prepare AAGBs, these two representative components were linked alternatively as pendent groups onto a polypeptide backbone prepared by condensation polymerization via our previous strategy.[39]

In order to explore the basic role of the complex amphiphilic structure in controlling its assembly morphologies, a small library of AAGBs has been constructed where the polymeric structure was tuned by three parameters, i.e., generations of the backbone dendrons, structure of the conjugated oligosaccharides, and number of the oligophenylalanine. We found that the resulting AAGBs self-assembled into various morphologies, including compound micelle, nanowire, nanoribbon, etc., mainly depending on the ratio of mannoside number in glycodendron and number of phenylalanine in oligophenylalanine component. Strong evidence showed that nanowires were formed from hierarchical self-assemble processes, i.e., the AAGBs first formed micelles, the micelles then further aligned into filaments, the filaments grew with branches via micelles, and finally the filaments fused into nanowires. This hierarchical self-assembly mechanism[40] has not been reported previously in any research on brush copolymers. Furthermore, the protein binding ability of different assembled morphologies was evaluated.

RESULT AND DISCUSSION

Design and Synthetic Strategies of Alternating Amphiphilic Glycopeptide Brushes (AAGBs). Very recently, we used metal-free step-growth copolymerization to prepare hybrid copolymers from oligopeptide blocks linked by small molecules.[39] In this paper, the same strategy has been employed. Briefly, the step-growth polymerization between

DOI: 10.1021/jacs.6b05044
J. Am. Chem. Soc. 2016, 138, 12387−12394

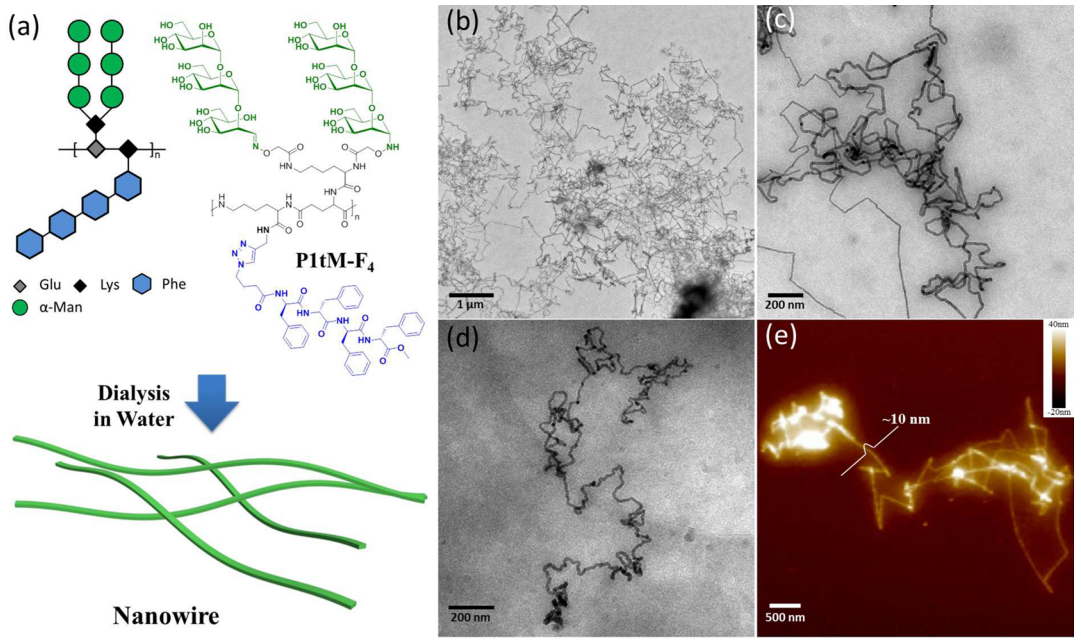

Figure 1. TEM and AFM images of the nanowires formed by **P1tM-F$_4$** in water, (a) chemical structure, and 2D schematic illustration of **P1tM-F$_4$**, (b, c) low/high-magnification TEM images, (d) cyro-TEM image, and (e) AFM image of the **P1tM-F$_4$** nanowires.

pentafluorophenol (PFp) active ester and primary amine functionalized monomer was used due to their high reactive efficiency under mild conditions (Scheme 1). PFp active ester functionalized monomer **M0**, **M1**, **M2** and amine-functionalized monomer **M-a** based on Lysine and Glutamate were first prepared separately via liquid phase peptide synthesis (synthetic details in the Supporting Information, Schemes S1−S5). Different generations of dendron scaffolds were attached to PFp active ester monomer as pendent groups. Then step-growth polymerization was performed by simply adding 1.2 equiv of *N*,*N*-diisopropyl ethylamine (DIPEA) to the equal molar mixture of **M-a** with **M0**, **M1**, or **M2** in DMSO at room temperature. The resulted viscous mixtures were allowed to precipitate in diethyl ether, giving alkyne-functionalized precursors. These precursors were deprotected in TFA and then modified with aminooxy monomer **M-b**, giving scaffolds **P0**, **P1**, and **P2** (Scheme 1). The aminooxy nucleophiles are introduced for their high reactivity with reducing saccharides under mild reaction conditions. Molar mass of **P0**, **P1**, and **P2** was measured by gel permeation chromatography with a multiangle light scattering detector (GPC-MALS) in DMF. **P0** and **P1** gave the molar mass of 18.9 kDa and 16.6 kDa, respectively, while the molar mass of **P2** can hardly be measured due to its poor solubility in DMF (molar mass of corresponding precursors were listed in Table S1,d*n*/d*c* measurement and GPC traces were shown in Figures S1−S6).

Then reducing saccharides were modified to aminooxy nucleophiles at the end of pendent dendron on scaffolds **P0**, **P1**, and **P2**. The experiments were performed in acetate buffer (200 mM, pH 3.5) with 100 mM aniline as the catalyst. Typically, the scaffolds with aminooxy groups (**P0**, **P1**, and **P2**) were dissolved in acetate buffer, after which 1.2 equiv of corresponding saccharides (Scheme 2, **M**, mannose; **dM**, Manα1-2Man; **tM**, Manα1-2Manα1-2Man) were added separately and the mixtures were kept at 40 °C. Relatively high conversion ratios of the aminooxy groups were obtained (80−95%, calculated from ^{1}H NMR, Table S2). Excess saccharides (2 equiv or more) were also used for this reaction but no obvious increment of the conversion rate was observed. According to the literature,[41] carbohydrate oxime O-ethers were formed during covalent coupling of reducing saccharides with aminooxy nucleophiles. The reaction normally generates more oxime rather than mannosylamine due to the higher chemical stability of the former. Accordingly, 12−15% of the ring-closed mannosylamine were found among the aminooxy glycosylation sites on the side chain (Table S2). For trimannoside-modified polypeptides **P0tM**, **P1tM**, and **P2tM**, the mannosylamine content cannot be determined from ^{1}H NMR due to signal overlapping with other anomeric ^{1}H signal and D_2O solvent residue. The molar mass of glycopolypeptides was measured by gel permeation chromatography with multiangle light scattering detector (GPC-MALS) in water (0.8% $NaNO_3$) and listed in Table S1.

The alkyne-functionalized backbone provided active sites for further postpolymerization modification (Scheme 2). Azide-modified oligophenylalanine **M-c** (**F$_2$**) and **M-d** (**F$_4$**) were synthesized as the hydrophobic domain for their known high tendency to form stable β-sheets. Modification of **M-c** or **M-d** was performed by typical Cu(I) catalyzed CuAAC reaction (or "click") in DMSO, resulting in AAGBs. A total of 5% of LiBr was added to increase the solubility of **M-c**/**M-d**. For example, after clicking with **M-d**, **P2tM** was transformed to **P2tM-F$_4$**.

A Representative Self-Assembly of AAGB P1tM-F$_4$. We first discuss the self-assembly of AAGB **P1tM-F$_4$** with medium sizes of hydrophilic and hydrophobic domains (Figure 1a). Typically, 2 mL water was added to 1 mL of clear DMSO solution of **P1tM-F$_4$** (30 mg/mL). Then the mixture was allowed to undergo dialysis against deionized water. Opalescence appeared suggesting formation of **P1tM-F$_4$** assemblies. After dialysis for 48 h, the solution was diluted to 2 mg/mL by adding deionized water. A large amount of long nanowires was observed by TEM (Figure 1b, c) with a uniform width around 25 nm. The length of each nanowire was hardly determined due to the entanglement of the wires, but obviously the length

DOI: 10.1021/jacs.6b05044
J. Am. Chem. Soc. 2016, 138, 12387−12394

Table 1. Sample Codes, 2D Illustrations, S/F Ratios, and the Assembled Morphologies of AAGBs Library

Sample codes	Morphology	S/F	2D illustrations	Sample codes	Morphology	S/F	2D illustrations
P0M-F_2	Precipitate	0.5		P0M-F_4	Precipitate	0.25	
P1M-F_2	Precipitate	1.0		P1M-F_4	Precipitate	0.5	
P2M-F_2	Nanowire	2.0		P2M-F_4	Precipitate	1.0	
P0dM-F_2	Precipitate	1.0		P0dM-F_4	Precipitate	0.5	
P1dM-F_2	Nanowire	2.0		P1dM-F_4	Nanoribbon	1.0	
P2dM-F_2	Compound Micelle	4.0		P2dM-F_4	Nanowire	2.0	
P0tM-F_2	Nanowire	1.5		P0tM-F_4	Precipitate	0.75	
P1tM-F_2	Compound Micelle	3.0		P1tM-F_4	Nanowire	1.5	
P2tM-F_2	Compound Micelle	6.0		P2tM-F_4	Nanowire	3.0	

was at least in the micrometer range. The nanowire morphology was further confirmed by cryo-TEM (Figure 1d). Also the image under atomic force microscope (AFM) suggested that the thickness of the nanowire was around 10 nm (Figure 1e, Figures S7 and S8). The nanowires inclined to entangle into large cluster at high concentration ([**P1tM-F_4**] > 1 mg/mL) in less than 7 days (Figure S9a), but they are quite stable for more than 30 days at a low concentration ([**P1tM-F_4**] < 0.2 mg/mL) at room temperature. We noticed that such long and uniform nanowires are rarely observed for the assemblies of amphiphilic block copolymers and polymeric brushes, which deserved further investigation in detail.

Self-Assembly of AAGB Library. To further explore the general rule of AAGB assembly with emphasis on the effects of glycodendron and oligophenylalanine brushes, a library of AAGBs was designed varying in dendritic-polypeptide scaffold (**P0**, **P1**, and **P2**), hydrophobic peptide domain (**F_2**/**F_4**) and oligomannoside domain (**M**, **dM**, and **tM**, Table 1). The same procedures as the mentioned for **P1tM-F_4** were used for the sample preparation and their assembly.

Generally, during the process of dialysis where the medium turned from hydrophobic to hydrophilic, the 18 samples showed very different responses: a great part of them, i.e., seven samples precipitated without any assembled structures. Three samples showed compound micelles, **P2dM-F_2**, **P1tM-F_2**, and **P2tM-F_2** (Figure 2a and Figure S9b,c). The nanowires, which were seldom found in synthetic copolymers and interested us most, became the common features of the samples including **P1dM-F_2**, **P2tM-F_4**, **P2M-F_2**, **P0tM-F_2**, and **P2dM-F_4** (Figure 2b,c and Figure S9d–f). Nanoribbon is a special case, obtained only from **P1dM-F_4** (Figure 2d). Different from the long and homogeneous nanowire, the nanoribbon was heterogeneous with its width distributed in the range of 50–100 nm. The ribbons were not stable and easy to precipitate in water. At first glance, such diversity of the morphologies observed seems not easy to be explained by relating the results to the structural parameters directly.

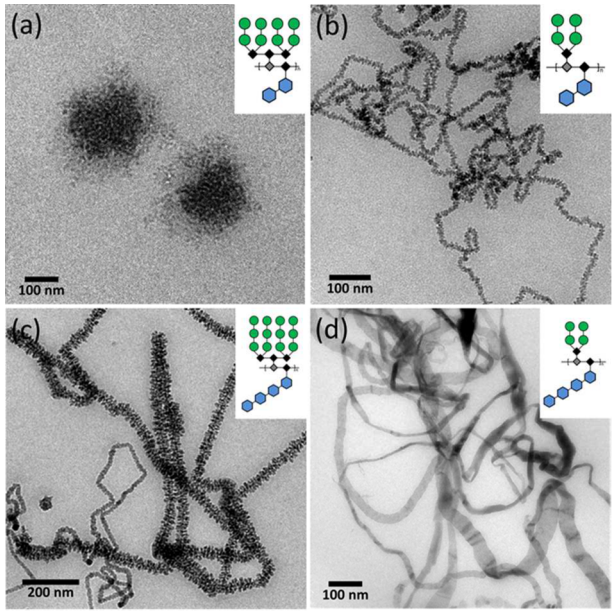

Figure 2. TEM images of (a) **P2dM-F_2** (compound micelle), (b) **P1dM-F_2** (nanowire), (c) **P2tM-F_4** (nanowire), and (d) **P1dM-F_4** (nanoribbon).

Although the architectures of our AAGB are complicated, we inclined to think that the hydrophobicity–hydrophilicity balance is still the main factor governing their behavior in self-assembly. Therefore, we simply introduced a parameter S/F, i.e., number ratio of saccharide units to phenylalanine monomer units in evaluating the assembly (Table 1). Thus, a "phase diagram" was constructed (Figure 3), in which the S/F ratio and the scaffolds character (**P0**, **P1**, and **P2**) serve the abscissa and ordinate axes, respectively. Fortunately, in the

DOI: 10.1021/jacs.6b05044
J. Am. Chem. Soc. 2016, 138, 12387–12394

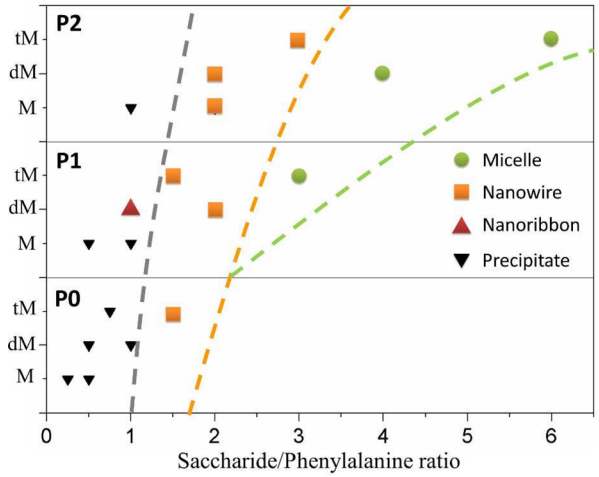

Figure 3. Phase diagram of AAGP assemblies depends on S/F ratio and different polypeptide scaffolds (**P0**, **P1**, and **P2**).

diagram, a clear relationship between the assembly behavior and the structural parameters of the library members displayed as follows. At low S/F ratios (≤1.0), precipitates or irregular aggregates appeared, probably because their relatively small hydrophilic domains failed to stabilize the aggregates in water. When the S/F ratio was increased to a much larger value (≥3.0), compound micelle became the major morphology, because of the large hydrophilic and small hydrophobic domains of the polymers in this area. When S/F exists in the small window of $1.5 \leq S/F \leq 3.0$, the nanowire was the only morphology observed. It was noticed that at the upper boundary value 3.0 of S/F ratio, stable nanowires were formed by **P2tM-F$_4$** with FFFF domain, while compound micelles were formed by **P1tM-F$_2$** with the FF domain, so the longer phenylalanine had stronger regular packing tendency leading to nanowires. In short, the self-assembled morphologies were generally controlled by the S/F ratio, i.e., precipitates, nanoribbon, nanowires, and compound micelles were sequentially observed, when the S/F ratio was increased.

Self-Assembly Mechanism of the AAGB Nanowires. The nanowire, which was found in the small S/F "window", deserves deep research because in previous self-assembly studies on the glycopolypeptide, either peptide as the main chain or pendent groups, the nanowire was rarely observed. However, in this work, nanowires can be formed for all kinds of the main chain peptide, i.e., **P0**, **P1**, and **P2** provided S/F exists in the window. Therefore, we tried to use electronic microscopy to trace the formation of the nanowires for understanding the mechanism. Nevertheless, formation of **P1tM-F$_4$** nanowires, as mentioned above was quite fast (within a couple of hours), it was almost not possible to capture stable intermediate states under TEM. Considering that S/F of **P2tM-F$_4$** (3.0) was much higher than that of **P1tM-F$_4$** (1.0), showing lower packing strength and slower assembly process and therefore, it was selected for this mechanical study. In addition, to further retard the process, a highly diluted solution (2 mg/

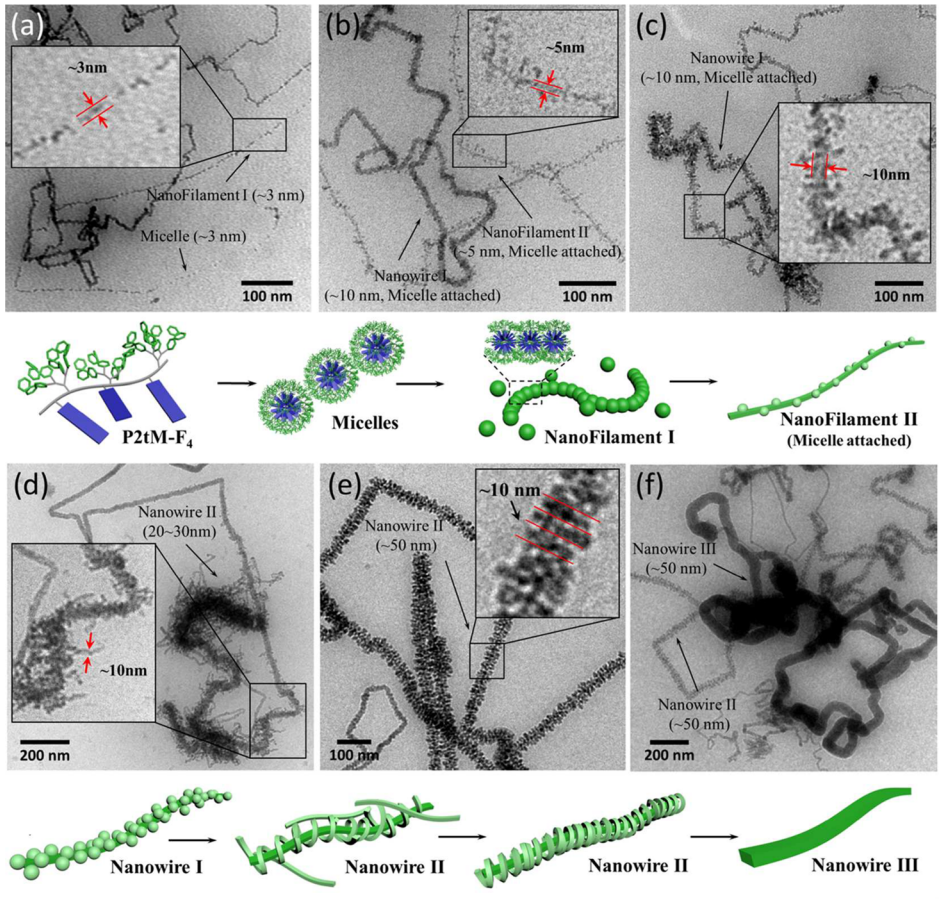

Figure 4. TEM images of the nanowires formed by the hierarchical self-assembly of **P2tM-F$_4$** and proposed self-assembly mechanism, the intermediate states captured from the samples prepared after (a) 3 h, (b, c) 12 h, (d) 24 h, and (e, f) 48 h dialysis.

DOI: 10.1021/jacs.6b05044
J. Am. Chem. Soc. 2016, 138, 12387−12394

mL) of **P2tM-F$_4$** was used for dialysis. Thus, the assembly process finished in about 2 days, which made the TEM sample preparation at different stages possible. Typically, at each time intervals of 3 h, 12 h, 24 h, and 48 h, a small aliquot of the solution was taken out and quenched by a large amount of water to "freeze" the intermediate morphology.

The TEM image of **P2tM-F$_4$** taken at 3 h (Figure 4a) was featured by the coexistence of micelles with a diameter around 3−5 nm and nanofilaments with the same width. It could be clearly seen that some of the small micelles were aligned and linked to strings, which obviously was the primary form of nanofilament (nanofilament I). When the dialysis time was increased to 12 h (Figure 4b), the nanofilaments could still be observed, but more micelles were found attaching to the surface of the nanofilaments, forming "branches" (nanofilament II). In the same stage (Figure 4c), thin nanowires (nanowire I) with a rough surface and a wider diameter (∼10 nm) compared to the primary nanofilaments were observed. These results indicated that the nanofilaments were partially transformed into nanowires via the growth of micelle "branch" on the filament surface. Meanwhile, at this stage, single micelles or micelle strings disappeared. Then from the sample taken at 24 h (Figure 4d), wide and compact nanowires with a diameter around 20−30 nm became the dominate morphology (nanowire II). "Branched" structure was also found on the surface of these nanowires, but here the "branch" turned to nanofilaments with a diameter around 10 nm. These attached filaments were found twisted on the stem of the nanowire. Finally, after 48 h (Figure 4e; Figures S10 and S11), these twisted nanofilament "branches" became regularly circling the wire with a period of 10 nm as shown in the inset of Figure 4e. A similar regular structure was also observed in the assemblies of **P1tM-F$_4$** under TEM (Figure S12) and of **P2tM-F$_4$** by the cryofixation sample preparation method (Figure S13). At the same time interval, thick and wide nanowires were also observed (Figure 4f, nanowire III, diameter ∼50 nm). Such thick nanowires became more uniform without inner structures as probably a result of fusion of the surrounding nanofilaments (Figure 4f; Figure S11).

Although the TEM studies could not trace the details of the whole hierarchical self-assembly process of AAGBs, the evolution outline of the morphologies has been clearly sketched. It becomes clear that the formation of the nanowires of AAGBs stems from the basic assemblies, i.e., the ordinary micelles of AAGBs formed due to their amphiphilicity. The following steps include the micelles alignment, formation of the nanofilaments, attachment of micelles to the filaments, formation of the nanowires due to the fusion of the attached micelles and finally, formation of the thick nanowire, etc. It is not difficult to realize that the key factor driving all the steps is the association between the sugar "shell" of the primary micelles,[42] as well as the subsequent assemblies including the nanofilaments, branches, and nanowires. Such hierarchical assembly has not been reported for other glycopolypeptides in the literature, probably because in our AAGBs, the coating hydrophilic layers of all of the assemblies at different levels consist of much high sugar density due to the dendron structure of the sugar pendants. The dense sugar shell might favor the alignment of micelles forming string or nanofilament, which became the second primary building block of the final nanowire. In our previous study,[43] we proposed that when two micelles of block copolymers fused to each other, the chain density of the shell on the two ends was lighter than that of the lateral sides, which would direct the next coming micelle to approach and attach to the two ends of the fused micelle. With the heavy glyco-dendron shell in the current case, the alignment of micelles could be explained by the same rationale. On the other hand, typical signal of β-sheet structure was observed among the nanowire samples including **P1tM-F$_4$**, **P2tM-F$_4$**, and **P2dM-F$_4$** by circular dichroism (CD) spectroscopy (Figure S14), so β-sheet packing is another driving force leading to nanowires. In contrast, CD spectra indicated that all compound micelles exhibit typical random coil secondary structure rather than the β-sheet, and the nanowires formed by AAGBs with the short peptide FF brushes show the same results (Figures S15 and S16). The result indicates that β-sheet forming tendency of oligophenylalanine is determined by the length of oligophenylalanine species and is affected by the dense sugar shell.

Effect of Morphologies of AAGB Assemblies on Their Binding Ability to Proteins. In nature, different morphologies sometimes simply indicate different functions of the assemblies. Herein, Human Immunodeficiency Virus (HIV) antibody 2G12 and plant lectin Concanavalin A (Con A) were chosen as models to evaluate the protein binding ability of the nanowires and compound micelles of AAGBs. 2G12 is a broadly neutralizing human monoclonal antibody (mAb), which can specifically recognize terminal Manα1-2Man moieties. First the binding ability of self-assembled AAGBs to 2G12 was evaluated by sandwich enzyme linked immunosorbent assay (ELISA). In this experiment, 2G12 was immobilized to the surface coated with gp120, a major envelope protein of HIV, which binds to 2G12 via the N-linked high mannose glycan on its surface.[44] Then inhibition of this binding by adding free oligosaccharides and self-assembled AAGBs, respectively, was evaluated by ELISA. As shown in Figure 5a, both Manα1-2Man (diMan), Manα1-2Manα1-2Man (triMan) and their corresponding assemblies showed significant inhibition for 2G12-carbohydrate recognition, while mannose (Man) and its corresponding assembly **P1M-F$_2$** did not. Furthermore, generally, compound micelles, e.g., **P2tM-F$_2$** showed higher inhibition ability to the binding between 2G12 and gp120 than nanowires, e.g., **P2tM-F$_4$** did. These two polymer brushes shared the same generation of dendron, same trisaccharide, but different morphologies and subsequently different binding ability. The same phenomenon was also observed between **P1tM-F$_2$** compound micelle and **P1tM-F$_4$** nanowire. This may due to the less steric hindrance in compound micelles than that in nanowires favoring the inhibition of the binding between 2G12 and oligosaccharides. Moreover, when plant lectin Con A was utilized, this trend was even more pronounced, as shown from the result of quantitative agglutination experiment[45] (Figure 5b), i.e., the compound micelles gave a higher binding ability to Con A than nanowires did, especially between **P2tM-F$_2$**/**P2tM-F$_4$** and **P1tM-F$_2$**/**P1tM-F$_4$**. These results might be explained by the different curvature of the nano-objects, i.e., higher curvature of micelles and lower ones of nanowires.

■ CONCLUSION

In this work, a hierarchical self-assembly process forming nanowires was observed in newly designed alternating amphiphilic glycopolypeptide brushes. Various self-assembled morphologies were achieved, including nanowires, nanoribbon, and compound micelles mainly depending on the number ratio of the sugar units to the amino acids species (S/F). We found that the glycopolypeptides first self-assembled into micelles

DOI: 10.1021/jacs.6b05044
J. Am. Chem. Soc. 2016, 138, 12387−12394

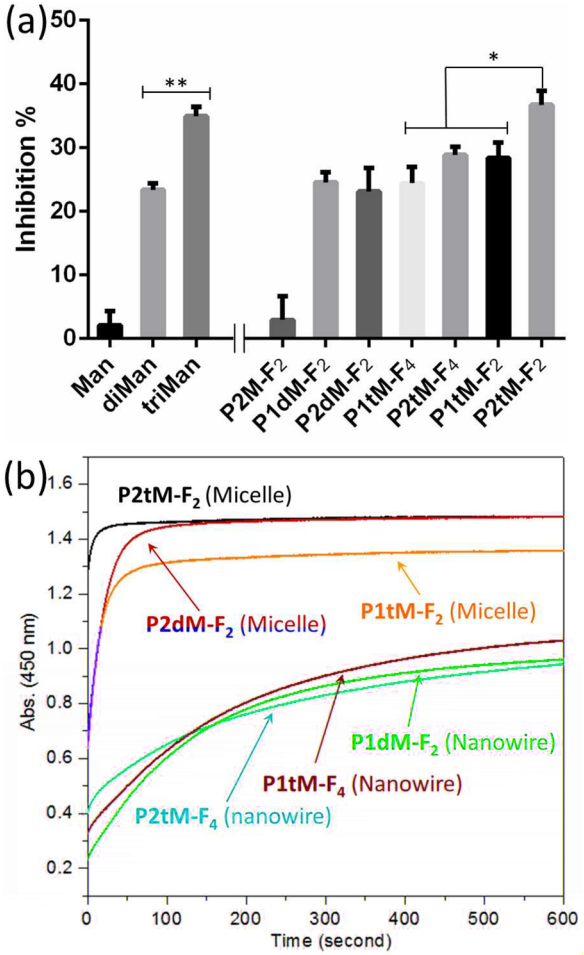

Figure 5. (a) ELISA analysis on 2G12-gp120 binding inhibition (%) by AAGB assemblies at mannose-residue concentration of 2 mM. (b) Qualitative agglutination of Con A with AAGB assemblies.

which became the basic building block forming nanofilaments. Then the nanofilaments grew into branches and finally fused into nanowires. This very interesting phenomenon has not been reported in the previous self-assembly of glycopolypeptide, polypeptide, and even polymer brushes. The result indicated that by using a dense layer of oligosaccharides, new self-assembly mechanism is possible, showing a bright future of glycopolypeptide in mimicking nature and developing new biocompatible materials. This newly synthesized AAGB architecture also brings us new thoughts in construction and the assembly mechanism of one-dimensional nanostructure.

■ ASSOCIATED CONTENT

Supporting Information

The Supporting Information is available free of charge on the ACS Publications website at DOI: 10.1021/jacs.6b05044.

Characterization of synthesized glycopolypeptide and corresponding precursors, including ^{1}HNMR and GPC results, dynamic light scattering, circular dichroism, TEM, AFM, as well as concentration dependent ELISA and UV agglutination results (PDF)

■ AUTHOR INFORMATION

Corresponding Author

*guosong@fudan.edu.cn

Notes

The authors declare no competing financial interest.

■ ACKNOWLEDGMENTS

National Natural Science Foundation of China (Grant Nos. 91527305, 21474020, 91227203, and 51322306) and the Innovation Program of the Shanghai Municipal Education Commission are acknowledged for their financial support.

■ REFERENCES

(1) (a) Pratt, M. R.; Bertozzi, C. R. *Chem. Soc. Rev.* **2005**, *34* (1), 58–68. (b) Bonduelle, C.; Lecommandoux, S. *Biomacromolecules* **2013**, *14* (9), 2973–2983.

(2) (a) Song, W. J.; Tzecan, F. A. *Science* **2014**, *346* (6216), 1525–1528. (b) Pati, D.; Kalva, N.; Das, S.; Kumaraswamy, G.; Sen Gupta, S.; Ambade, A. V. *J. Am. Chem. Soc.* **2012**, *134* (18), 7796–7802. (c) Huang, J.; Bonduelle, C.; Thevenot, J.; Lecommandoux, S.; Heise, A. *J. Am. Chem. Soc.* **2012**, *134* (1), 119–122.

(3) Ladmiral, V.; Semsarilar, M.; Canton, I.; Armes, S. P. *J. Am. Chem. Soc.* **2013**, *135* (36), 13574–13581.

(4) Hudak, J. E.; Canham, S. M.; Bertozzi, C. R. *Nat. Chem. Biol.* **2013**, *10* (1), 69–75.

(5) Svajger, U.; Anderluh, M.; Jeras, M.; Obermajer, N. *Cell. Signalling* **2010**, *22* (10), 1397–1405.

(6) Wang, L.-X. *Curr. Opin. Chem. Biol.* **2013**, *17* (6), 997–1005.

(7) Galan, M. C.; Dumy, P.; Renaudet, O. *Chem. Soc. Rev.* **2013**, *42* (11), 4599–4612.

(8) (a) Kramer, J. R.; Deming, T. J. *J. Am. Chem. Soc.* **2010**, *132* (42), 15068–71. (b) Kramer, J. R.; Deming, T. J. *J. Am. Chem. Soc.* **2012**, *134* (9), 4112–4115.

(9) (a) Shaikh, A. Y.; Das, S.; Pati, D.; Dhaware, V.; Sen Gupta, S.; Hotha, S. *Biomacromolecules* **2014**, *15* (10), 3679–3686. (b) Zhang, Q.; Su, L.; Collins, J.; Chen, G.; Wallis, R.; Mitchell, D. A.; Haddleton, D. M.; Becer, C. R. *J. Am. Chem. Soc.* **2014**, *136* (11), 4325–4332.

(10) Bonduelle, C.; Huang, J.; Ibarboure, E.; Heise, A.; Lecommandoux, S. *Chem. Commun.* **2012**, *48* (67), 8353–8355.

(11) Krannig, K. S.; Schlaad, H. *Soft Matter* **2014**, *10* (24), 4228–35.

(12) Huang, J.; Heise, A. *Chem. Soc. Rev.* **2013**, *42* (17), 7373–7390.

(13) (a) Jacobs, J.; Gathergood, N.; Heuts, J. P. A.; Heise, A. *Polym. Chem.* **2015**, *6* (25), 4634–4640. (b) Schatz, C.; Louguet, S.; Le Meins, J. F.; Lecommandoux, S. *Angew. Chem., Int. Ed.* **2009**, *48* (14), 2572–2575.

(14) Bonduelle, C.; Huang, J.; Mena-Barragan, T.; Ortiz Mellet, C.; Decroocq, C.; Etame, E.; Heise, A.; Compain, P.; Lecommandoux, S. *Chem. Commun.* **2014**, *50* (25), 3350–3352.

(15) (a) Krannig, K. S.; Schlaad, H. *J. Am. Chem. Soc.* **2012**, *134* (45), 18542–18545. (b) Krannig, K. S.; Sun, J.; Schlaad, H. *Biomacromolecules* **2014**, *15* (3), 978–84. (c) Mildner, R.; Menzel, H. *Biomacromolecules* **2014**, *15* (12), 4528–4533.

(16) Pati, D.; Das, S.; Patil, N. G.; Parekh, N.; Anjum, D. H.; Dhaware, V.; Ambade, A. V.; Sen Gupta, S. *Biomacromolecules* **2016**, *17* (2), 466–475.

(17) (a) Bonduelle, C.; Huang, J.; Ibarboure, E.; Heise, A.; Lecommandoux, S. *Chem. Commun.* **2012**, *48* (67), 8353–8355. (b) Bonduelle, C.; Mazzaferro, S.; Huang, J.; Lambert, O.; Heise, A.; Lecommandoux, S. *Faraday Discuss.* **2013**, *166*, 137. (c) Das, S.; Pati, D.; Tiwari, N.; Nisal, A.; Sen Gupta, S. *Biomacromolecules* **2012**, *13* (11), 3695–3702.

(18) (a) Zepon, K. M.; Otsuka, I.; Bouilhac, C.; Muniz, E. C.; Soldi, V.; Borsali, R. *Biomacromolecules* **2015**, *16* (7), 2012–2024. (b) Das, S.; Sharma, D. K.; Chakrabarty, S.; Chowdhury, A.; Sen Gupta, S. *Langmuir* **2015**, *31* (11), 3402–3412. (c) Kramer, J. R.; Rodriguez, A. R.; Choe, U.-J.; Kamei, D. T.; Deming, T. J. *Soft Matter* **2013**, *9* (12), 3389–3395.

(19) Huang, Z.; Fang, Y.; Luo, Q.; Liu, S.; An, G.; Hou, C.; Lang, C.; Xu, J.; Dong, Z.; Liu, J. *Chem. Commun.* **2016**, *52* (10), 2083–2086.

(20) Hu, X.; Liu, G.; Li, Y.; Wang, X.; Liu, S. *J. Am. Chem. Soc.* **2015**, *137* (1), 362–368.

DOI: 10.1021/jacs.6b05044
J. Am. Chem. Soc. 2016, 138, 12387–12394

(21) Borase, T.; Ninjbadgar, T.; Kapetanakis, A.; Roche, S.; O'Connor, R.; Kerskens, C.; Heise, A.; Brougham, D. F. *Angew. Chem., Int. Ed.* **2013**, *52* (11), 3164−3167.
(22) Grieshaber, S. E.; Farran, A. J.; Bai, S.; Kiick, K. L.; Jia, X. *Biomacromolecules* **2012**, *13* (6), 1774−1786.
(23) Feng, C.; Li, Y.; Yang, D.; Hu, J.; Zhang, X.; Huang, X. *Chem. Soc. Rev.* **2011**, *40* (3), 1282−1295.
(24) Zhang, M.; Liu, H.; Shao, W.; Miao, K.; Zhao, Y. *Macromolecules* **2013**, *46* (4), 1325−1336.
(25) Ping, J.; Qiao, Y.; Tian, H.; Shen, Z.; Fan, X.-H. *Macromolecules* **2015**, *48* (3), 592−599.
(26) Zhang, Z.; Hong, L.; Li, J.; Liu, F.; Cai, H.; Gao, Y.; Zhang, W. *RSC Adv.* **2015**, *5* (28), 21580−21587.
(27) Palmer, L. C.; Leung, C. Y.; Kewalramani, S.; Kumthekar, R.; Newcomb, C. J.; Olvera de la Cruz, M.; Bedzyk, M. J.; Stupp, S. I. *J. Am. Chem. Soc.* **2014**, *136* (41), 14377−14380.
(28) Pazos, E.; Sleep, E.; Rubert Perez, C. M.; Lee, S. S.; Tantakitti, F.; Stupp, S. I. *J. Am. Chem. Soc.* **2016**, *138* (17), 5507−5510.
(29) Wang, J.; Liu, K.; Yan, L.; Wang, A.; Bai, S.; Yan, X. *ACS Nano* **2016**, *10* (2), 2138−2143.
(30) (a) Blum, A. P.; Kammeyer, J. K.; Yin, J.; Crystal, D. T.; Rush, A. M.; Gilson, M. K.; Gianneschi, N. C. *J. Am. Chem. Soc.* **2014**, *136* (43), 15422−15437. (b) Wu, L.-y.; Yu, L.; Fu, X.-h.; Li, Z.-b. *Chin. J. Polym. Sci.* **2015**, *33* (8), 1140−1149.
(31) Conrad, R. M.; Grubbs, R. H. *Angew. Chem., Int. Ed.* **2009**, *48* (44), 8328−8330.
(32) (a) Yu, Z.; Tantakitti, F.; Yu, T.; Palmer, L. C.; Schatz, G. C.; Stupp, S. I. *Science* **2016**, *351* (6272), 497−502. (b) Wang, Z.; Li, Y.; Huang, Y.; Thompson, M. P.; LeGuyader, C. L.; Sahu, S.; Gianneschi, N. C. *Chem. Commun.* **2015**, *51* (96), 17108−17111.
(33) Carvalho de Souza, A.; Halkes, K. M.; Meeldijk, J. D.; Verkleij, A. J.; Vliegenthart, J. F.; Kamerling, J. P. *ChemBioChem* **2005**, *6* (5), 828−831.
(34) Zeng, H.; Little, H. C.; Tiambeng, T. N.; Williams, G. A.; Guan, Z. *J. Am. Chem. Soc.* **2013**, *135* (13), 4962−4965.
(35) Horiya, S.; MacPherson, I. S.; Krauss, I. J. *Nat. Chem. Biol.* **2014**, *10* (12), 990−999.
(36) Horiya, S.; Bailey, J. K.; Temme, J. S.; Guillen Schlippe, Y. V.; Krauss, I. J. *J. Am. Chem. Soc.* **2014**, *136* (14), 5407−5415.
(37) Reches, M.; Gazit, E. *Science* **2003**, *300* (5619), 625−627.
(38) (a) Wang, Y.; Qi, W.; Huang, R.; Yang, X.; Wang, M.; Su, R.; He, Z. *J. Am. Chem. Soc.* **2015**, *137* (24), 7869−7880. (b) Ikeda, M.; Tanida, T.; Yoshii, T.; Kurotani, K.; Onogi, S.; Urayama, K.; Hamachi, I. *Nat. Chem.* **2014**, *6* (6), 511−518. (c) Jones, B. H.; Martinez, A. M.; Wheeler, J. S.; McKenzie, B. B.; Miller, L. L.; Wheeler, D. R.; Spoerke, E. D. *Chem. Commun.* **2015**, *51* (77), 14532−14535.
(39) Liu, Y.; Kang, Y.; Wang, J.; Wang, Z.; Chen, G.; Jiang, M. *Biomacromolecules* **2015**, *16* (12), 3995−4003.
(40) Hu, Y.; Lin, R.; Zhang, P.; Fern, J.; Cheetham, A. G.; Patel, K.; Schulman, R.; Kan, C.; Cui, H. *ACS Nano* **2016**, *10* (1), 880−888.
(41) Thygesen, M. B.; Munch, H.; Sauer, J.; Clo, E.; Jorgensen, M. R.; Hindsgaul, O.; Jensen, K. J. *J. Org. Chem.* **2010**, *75* (5), 1752−1755.
(42) Majoinen, J.; Haataja, J. S.; Appelhans, D.; Lederer, A.; Olszewska, A.; Seitsonen, J.; Aseyev, V.; Kontturi, E.; Rosilo, H.; Osterberg, M.; Houbenov, N.; Ikkala, O. *J. Am. Chem. Soc.* **2014**, *136* (3), 866−869.
(43) (a) Peng, H.; Chen, D.; Jiang, M. *Macromolecules* **2005**, *38* (9), 3550−3553. (b) Wei, K.; Su, L.; Chen, G.; Jiang, M. *Polymer* **2011**, *52* (16), 3647−3654.
(44) Calarese, D. A.; Lee, H. K.; Huang, C. Y.; Best, M. D.; Astronomo, R. D.; Stanfield, R. L.; Katinger, H.; Burton, D. R.; Wong, C. H.; Wilson, I. A. *Proc. Natl. Acad. Sci. U. S. A.* **2005**, *102* (38), 13372−13377.
(45) Zhang, S.; Xiao, Q.; Sherman, S. E.; Muncan, A.; Ramos Vicente, A. D.; Wang, Z.; Hammer, D. A.; Williams, D.; Chen, Y.; Pochan, D. J.; Vertesy, S.; Andre, S.; Klein, M. L.; Gabius, H. J.; Percec, V. *J. Am. Chem. Soc.* **2015**, *137* (41), 13334−13344.

DOI: 10.1021/jacs.6b05044
J. Am. Chem. Soc. 2016, 138, 12387−12394